Optics Communications 453 (2019) 124322

Contents lists available at ScienceDirect

Optics Communications

journal homepage: www.elsevier.com/locate/optcom

High-SNR snapshot multiplex spectrometer with sub-Hadamard-S matrix coding

Zhuang Zhao [a], Lianfa Bai [a], Jing Han [a], Jiang Yue [b,*]

[a] School of Electronic Engineering and Optoelectronic Technology, Nanjing University of Science and Technology, Nanjing 210094, China
[b] National Key Laboratory of Transient Physics, Nanjing University of Science and Technology, Nanjing 210094, China

ARTICLE INFO

Keywords:
Spectrometer
Snapshot Hadamard transform spectrometer
Spectrum
Coded aperture

ABSTRACT

We present a robust high signal-to-noise ratio (SNR) snapshot multiplex spectrometer with sub-Hadamard-S matrix coding. Traditional Hadamard Transform Spectrometer (HTS) must vary the coding mask to obtain a reliable spectrum result, causing unexpected time consumption. Unlike traditional HTS, the proposed snapshot spectrometer comprises two imaging paths: non-dispersive and dispersive imaging paths; the additional non-dispersive imaging path is used to capture the light intensity of the coded aperture. Both light intensity of the coded aperture as well as the overlapped spectra are captured within one shot, turning Hadamard-S matrix coding into sub-Hadamard-S matrix coding. The simulated and experimental results obtained demonstrate for the first time that compared to Hadamard-S matrix used in HTS, the sub-Hadamard-S matrix could achieve similar SNR improvement and denoising capacity as well as maintain snapshot.

1. Introduction

A spectrometer is an extensively used tool in scientific and medical research. The accuracy of the measured spectra may be compromised by a weak source or transient phenomena; occasionally, a few research areas such as laser-matter interaction involve both: a weak source and transient phenomenon. There two remarkable technologies are proposed to address the spectrum measurement of a weak source: Hadamard transform spectroscopy (HTS) and Fourier Transform Spectroscopy (FTS). However, the measurement process employing these techniques is cumbersome and requires several additional measurements to achieve the desired signal-to-noise ratio (SNR); particularly, when a weak source as well as transient phenomenon are involved. A rapid and reliable snapshot measurement spectrometer with a high SNR is desired in such cases. Moreover, as a measurement tool, reliable improvement is crucial, which means it should exhibit a certain SNR improvement lower bound.

To realize high throughput advantages within a snapshot, several designs and methods based on compressive sensing (CS) [1–6], computational slits [7,8], and deconvolution [9] have been proposed. These methods try to improve the SNR and resolution of the spectrum via numerical methods. However, compared with the coding aperture, the numerical methods belong to the well-known ill-posed inverse problems; thus, the estimated results depend on the algorithms employed, the structure of the measured signal and, the type of noise, which means it cannot obtain certain and robust SNR improvement. The traditional multiplexing methods, such as HTS [10–12], have exhibited significant improvement in SNR. In particular, the SNR boost would increase along with the scale of the coding matrix [13–15]. However, the traditional multiplexing causes unexpected time consumption. A spectrometer with a certain and continuous SNR boost, maintaining snapshot, would enormously extend the applications of the spectrometer.

Among difference types of coding matrix, Hadamard-S matrix is well-structured and easy to implement. Moreover, it is the predominantly used coding matrix in multiplexing. Wagadarikar et al. proposed a compact and static multimodal multiplex spectrometer (MMS) based on this matrix [16]. In MMS, the non-negative least-squares (NNLS) method with the CS [16–18] is employed to reconstruct the spectrum of the scene, which maintains a high throughput and snapshot measurement. MMS has a compact optical structure and can obtain high SNR measured results; however, in MMS the light intensity is represented by coding matrix, causing unstable reconstructed results. To overcome this drawback, a dual-camera coded aperture snapshot spectral imaging is proposed [19]. The authors add an additional imaging path to detect the light intensity and then use a two-step iterative shrinkage/thresholding (TwIST) [20] to obtain the results. However, according to the theory of CS, the accuracy of the reconstructed result depends on the structure measured signal and the accuracy of the results is still inconsistent.

In this paper, we introduce a new coding matrix called sub-Hadamard-S matrix (sub-S matrix), which exhibits SNR improvement

* Corresponding author.
E-mail address: 190281182@qq.com (J. Yue).

https://doi.org/10.1016/j.optcom.2019.124322
Received 22 January 2019; Received in revised form 29 July 2019; Accepted 30 July 2019
Available online 8 August 2019

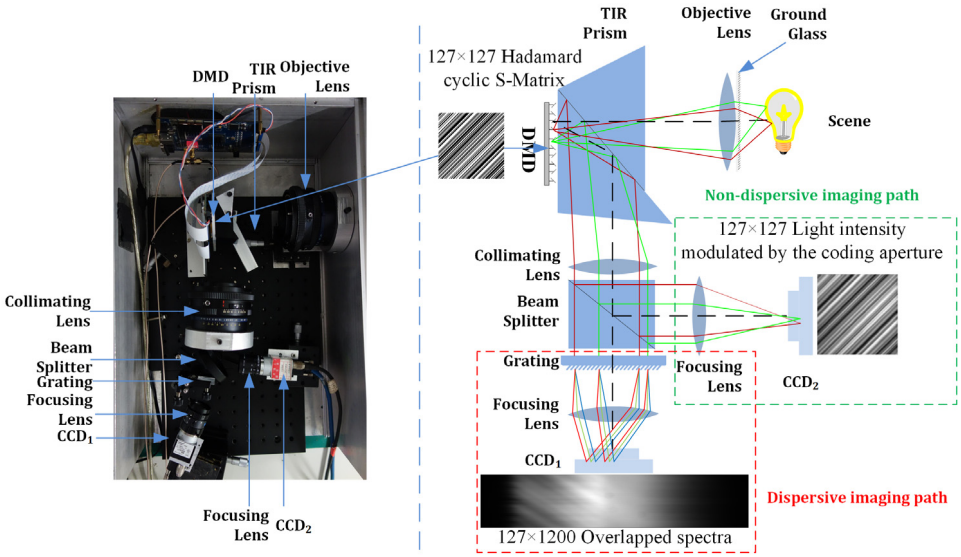

Fig. 1. Overview of the snapshot multiplexing spectrometer. (a) Implementation of the system. (b) Schematic of the implementation.

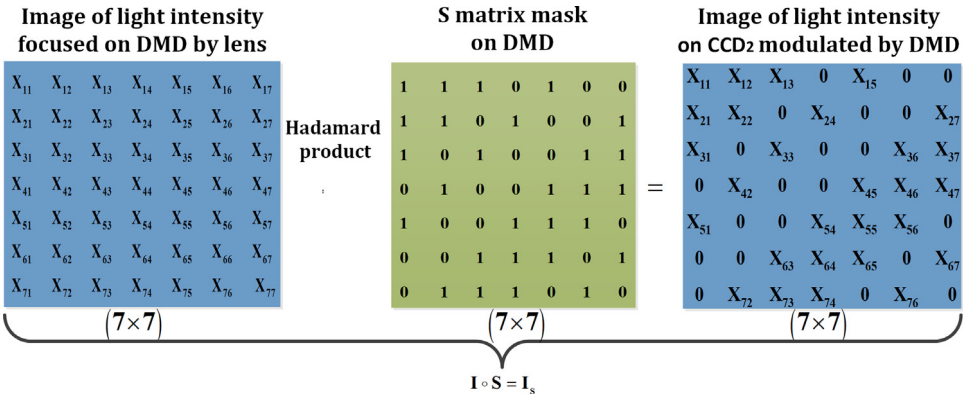

Fig. 2. Coding process in non-dispersive light path.

comparable to that of HTS and maintains snapshot. The proposed method contains two imaging paths: non-dispersive and dispersive imaging paths. The non-dispersive imaging path is employed to capture the light intensity at the coding aperture. The dispersive imaging path is employed to capture the overlapped dispersive spectra. Owing to the variation of the light intensity at the aperture, the standard Hadamard-S matrix would be turned into a sub-Hadamard-S matrix. We demonstrated that the sub-Hadamard-S matrix coding could realize a proximity denoising capability with the Hadamard-S matrix coding. Most importantly, it could provide a useful tool for the spectrum detection with transient and weak signals.

2. Implementation of snapshot multiplex spectrometer

The implementation and scheme of the proposed snapshot spectrometer with sub-Hadamard-S matrix are shown in Fig. 1(a) and (b), respectively. In the implementation, Hadamard-S matrix is employed to code the light at the aperture. A beam splitter (split ratio, 70:30) is utilized to split the beam into two paths. One is reformed to detect the light intensity distribution of the aperture, which is employed to retrieve the coding matrix, called non-dispersive imaging path. The measured results would be a sub-Hadamard-S matrix, as the light intensity of pixels would not be similar. The second beam from the splitter is dispersed by the blazed grating and the spectra of different pixels is re-formed at the aperture. The system contains two Charge Coupled Devices (CCDs) that work simultaneously and can be controlled through the synchronizing signal of the Digital Micromirror Device (DMD). The CCD_1 is employed to collect the overlapped dispersed spectra and CCD_2 is employed to collect the non-dispersed image of the aperture on DMD. The ground glass is employed to ensure uniform light intensity. The DMD (ED01N) has a resolution of 1024 × 768 and the pixel size of 13.68 μm ×13.68 μm. The CCD (Basler acA1920-155 μm) has a resolution of 1920 × 1200 and the pixel size of 5.86 μm ×5.86 μm.

The non-dispersive imaging path is easy to understand as solely mirror reflection and focused lens are involved. The light intensity will be modulated by the coding aperture (Hadamard-S matrix) on DMD. Taking the 7 × 7 Hadamard-S matrix as an example, Fig. 2 shows the coding process.

By using suitable focal length lens, we can ensure that each pixel of DMD is imaged by one or more pixels of the camera. Then, we use the method presented by Gao et al. [21] to extract the light intensity of the scene. Without the non-dispersive imaging path, the implementation of snapshot HTS is similar to a traditional HTS (Fig. 3), and its measurement process [4,16–18] can be given as follows:

$$\mathbf{C}=\mathbf{S}(\mathbf{I}\circ\mathbf{f}) \tag{1}$$

where, **S** is the coding matrix, **I** is the light intensity, "∘" denotes the Hadamard product operation, **f** is the spectra to be measured, and **C** is the measured overlapped spectra. In traditional HTS, the measured spectrum is modulated by the light intensity.

The traditional HTS requires *n*-measurements to reconstruct the spectrum and obtains reliable SNR improvement, where *n* is the order

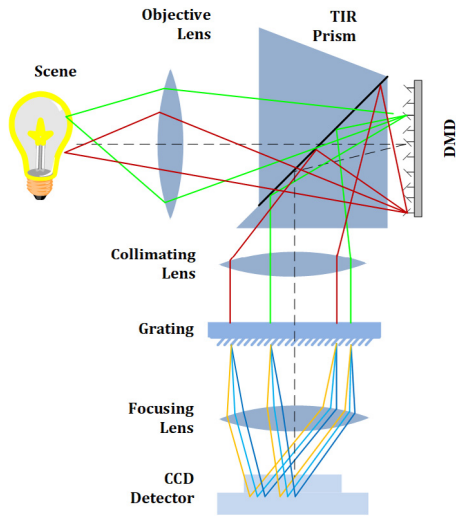

Fig. 3. Dispersive imaging path.

of coding matrix; therefore, this process is cumbersome for transient applications. In the snapshot HTS, the light intensity distribution of the aperture is modulated by the coding matrix as $\mathbf{I_S}$=S∘**I**. We map the whole coding matrix (Hadamard-S matrix) on the DMD to encode all the spectra. Based on our previous works [9,13,15], we take 7 × 7 Hadamard-S matrix as an example to explain the physical mechanism and mathematical expression of snapshot HTS in Fig. 4.

In Fig. 4, $\mathbf{S}^1$ is the first row of the Hadamard-S matrix, $\mathbf{I}_1$ is the first row of the light intensity distribution of the scene, $\mathbf{f}_1$ is the spectrum of the first row of the scene, $\mathbf{f}_{11}$ is the spectrum of the first pixel in the first row, and m represents its range. The zeros in the spectrum represent the shift invariant that make the process easy to understand. The measurement process of the ith row of the snapshot HTS is given as:

$$\mathbf{g}_i = (\mathbf{S}^i \circ \mathbf{I}_i)\mathbf{f}_i + \mathbf{n}_{\mathbf{snap}_i} \tag{2}$$

where, $\mathbf{g}_i$ is the overlapped dispersed spectra of ith row spectra, $\mathbf{S}^i$ is the ith row of Hadamard-S matrix, $\mathbf{I}_i$ is the ith row of the light intensity distribution **I**, $\mathbf{f}_i$ is the ith row spectra to be measured, $\mathbf{n}_{\mathbf{snap}_i}$ is the measurement noise in ith row measurement. If the light intensity at each element of the coding aperture is exactly the same, the normalized intensity of **I** can be treated as a standard Hadamard-S matrix, given by $\mathbf{S} = \mathbf{I}/\max(\mathbf{I}) = \mathbf{S}_{\mathrm{snap}}$. However, if the intensity of light is not the same at each element of the coding aperture, the $\mathbf{S}_{\mathrm{snap}}$ is treated as a sub-Hadamard-S matrix (sub S-matrix). Specifically, the $\mathbf{S}_{\mathrm{snap}}$ follows the condition: $0 \le \mathbf{S}_{\mathrm{snap}}(\mathrm{i},\mathrm{j}) \le 1, \{\mathrm{i} \le \mathrm{n}, \mathrm{j} \le \mathrm{n}\}$. If we want to measure the spectrum of a diffuse source, or the spectra of the source along the non-dispersive direction are slow varying or constant, i.e., $\mathbf{f}_1 = \mathbf{f}_2 = \cdots = \mathbf{f}_n$ or $\mathbf{f}_{11} = \mathbf{f}_{21} = \cdots = \mathbf{f}_{n1} = \frac{1}{n}\sum_{i=1}^{n}\mathbf{f}_{i1}$. Based on this acceptable assumption, the measurement of snapshot HTS can be simplified as:

$$\mathbf{g} = (\mathbf{S}\circ\mathbf{I})\,\mathbf{f} + \mathbf{n}_{\mathbf{snap}} = \mathbf{S}_{\mathbf{snap}}\mathbf{f} + \mathbf{n}_{\mathbf{snap}} = (\mathbf{S} - \mathbf{S}_1)\,\mathbf{f} + \mathbf{n}_{\mathbf{snap}} \tag{3}$$

where, $\mathbf{S}_1$ is the difference between Hadamard-S matrix **S** and the normalized modulated light intensity distribution $\mathbf{S}_{\mathrm{snap}}$, which satisfies the condition $0 \le \mathbf{S}_1(\mathrm{i},\mathrm{j}) < 1$.

Unlike NNLS, the problem of the snapshot HTS is a well-defined problem that helps in achieving a definite and stable SNR boost. In the next section, we will analyze the SNR boost of the snapshot HTS in further detail.

3. SNR analysis

In this section, we compare the denoising capacity of the sub S-matrix and the Hadamard-S matrix. First, the restored spectrum $\hat{\mathbf{f}}$ can be written as:

$$\hat{\mathbf{f}} = \mathbf{f} + (\mathbf{S} - \mathbf{S}_1)^{-1}\,\mathbf{n}_{\mathrm{snap}} \tag{4}$$

Then, the SNR boost of (**S**-$\mathbf{S}_1$) can be given as:

$$\begin{aligned} SNR_{\hat{\mathbf{f}}} &= 10\log\left(\frac{\mathbf{f}^T\mathbf{f}}{\mathbf{n}_{\mathrm{snap}}^T\left(\mathbf{S}^T-\mathbf{S}_1^T\right)^{-1}(\mathbf{S}-\mathbf{S}_1)^{-1}\mathbf{n}_{\mathrm{snap}}} \Big/ \frac{\mathbf{f}^T\mathbf{f}}{\mathbf{n}_{\mathrm{snap}}^T\mathbf{n}_{\mathrm{snap}}}\right) \\ &= 10\log\left(\frac{\mathbf{n}_{\mathrm{snap}}^T\mathbf{n}_{\mathrm{snap}}}{\mathbf{n}_{\mathrm{snap}}^T\left(\mathbf{S}^T-\mathbf{S}_1^T\right)^{-1}(\mathbf{S}-\mathbf{S}_1)^{-1}\mathbf{n}_{\mathrm{snap}}}\right) \end{aligned} \tag{5}$$

Using $\mathbf{n}'_{\mathrm{snap}} = (\mathbf{S}-\mathbf{S}_1)^{-1}\,\mathbf{n}_{\mathrm{snap}}$, then Eq. (5) can be rewritten as:

$$\begin{aligned} SNR_{\hat{\mathbf{f}}} &= 10\log\left(\frac{\mathbf{n}_{\mathrm{snap}}^T\mathbf{n}_{\mathrm{snap}}}{\mathbf{n}_{\mathrm{snap}}^T\left(\mathbf{S}^T-\mathbf{S}_1^T\right)^{-1}(\mathbf{S}-\mathbf{S}_1)^{-1}\mathbf{n}_{\mathrm{snap}}}\right) \\ &= 10\log\left(\frac{\left(\mathbf{n}'_{\mathrm{snap}}\right)^T\left(\mathbf{S}^T\mathbf{S}-\mathbf{S}^T\mathbf{S}_1-\mathbf{S}_1^T\mathbf{S}+\mathbf{S}_1^T\mathbf{S}_1\right)\mathbf{n}'_{\mathrm{snap}}}{\left(\mathbf{n}'_{\mathrm{snap}}\right)^T\mathbf{n}'_{\mathrm{snap}}}\right) \end{aligned} \tag{6}$$

If the minimum non-zero value in $\mathbf{S}_{snap}$ is α, the larger α, the smoother the distribution of light intensity. Thus, $\mathbf{S}_{\mathrm{snap}}$ can be rewritten as $\mathbf{S}_{\mathrm{snap}} = \alpha\mathbf{S} + \mathbf{S}_2$, where $\mathbf{S}_2$ is the difference between α**S** and $\mathbf{S}_{\mathrm{snap}}$. Then, we obtain $\mathbf{S} - \mathbf{S}_1 = \alpha\mathbf{S} + \mathbf{S}_2$, $(1-\alpha)\mathbf{S} = \mathbf{S}_1 + \mathbf{S}_2$, and $k\mathbf{S} = \mathbf{S}_1 + \mathbf{S}_2$, where $k = 1-\alpha$, is the disturbance of light intensity at the coding aperture. As noted previously, $\mathbf{S}_1$ satisfies $0 \le \mathbf{S}_1(i,j) < 1$. Using $0 \le \mathbf{S}_2(i,j) \le k$, $0 \le k < 1$, Eq. (6) can be written as:

$$SNR_{\hat{\mathbf{f}}} = 10\log\left(\frac{\left(\mathbf{n}'_{\mathrm{snap}}\right)^T\left((1-k)^2\,\mathbf{S}^T\mathbf{S} + \frac{1-k}{k}\mathbf{P}\right)\mathbf{n}'_{\mathrm{snap}}}{\left(\mathbf{n}'_{\mathrm{snap}}\right)^T\mathbf{n}'_{\mathrm{snap}}}\right) \tag{7}$$

where, $\mathbf{P} = \mathbf{S}_1^T\mathbf{S}_2 + \mathbf{S}_2^T\mathbf{S}_1 + (2-k)/(1-k)\,\mathbf{S}_2^T\mathbf{S}_2$. According to Eq. (7), $SNR_{\hat{\mathbf{f}}}$ strongly depends on the $\left(\mathbf{n}'_{\mathrm{snap}}\right)^T\mathbf{P}\mathbf{n}'_{\mathrm{snap}}$. To further estimate $\left(\mathbf{n}'_{\mathrm{snap}}\right)^T\mathbf{P}\mathbf{n}'_{\mathrm{snap}}$, we assume that the noise $\mathbf{n}_{\mathrm{snap}}$ is independent of random coding matrix $\mathbf{S}_1$, so is the $\mathbf{n}'_{\mathrm{snap}}$. Considering$\mathbf{S}_2 = k\mathbf{S} - \mathbf{S}_1$, $\mathbf{S}_1$ and $\mathbf{S}_2$ follow the same distribution; therefore, $\mathbf{n}_{\mathrm{snap}}$ is independent of $\mathbf{S}_2$. Hence, the following conclusions can be drawn based on the assumption:

$$\begin{aligned} &\mathrm{cov}\left(\mathbf{S}_1(1,j), \mathbf{n}'_{\mathrm{snap}}\right) \approx 0 \\ &\textstyle\sum_{j=1}^{n}\left(\mathbf{S}_1(1,j)\times\mathbf{n}'_{\mathrm{snap}}(j)\right) \propto E\left(\mathbf{S}_1(1,j)\right)\times E\left(\mathbf{n}'_{\mathrm{snap}}(j)\right) \\ &\left(\mathbf{n}'_{\mathrm{snap}}\right)^T\mathbf{S}_1^T\mathbf{S}_1\mathbf{n}'_{\mathrm{snap}} \propto \textstyle\sum_{k=1}^{n}\left\{E\left(\mathbf{S}_1(k,j)\right)\times E\left(\mathbf{n}'_{\mathrm{snap}}(j)\right)\right\}^2 \end{aligned} \tag{8}$$

Because $\mathbf{S}_1$ and $\mathbf{S}_2$ follow the same distribution, the mean of $\mathbf{S}_1(k,x)$ and $\mathbf{S}_2(k,x)$will be approximately the same, which can be given as:

$$E\left(\mathbf{S}_1(k,x)\right) \approx E\left(\mathbf{S}_2(k,x)\right) \tag{9}$$

Based on Eqs. (8) and (9), we can estimate that $\left(\mathbf{n}'_{\mathrm{snap}}\right)^T\mathbf{S}_1^T\mathbf{S}_1\mathbf{n}'_{\mathrm{snap}}$ and $\left(\mathbf{n}'_{\mathrm{snap}}\right)^T\mathbf{S}_2^T\mathbf{S}_2\mathbf{n}'_{\mathrm{snap}}$ will have the same values approximately:

$$\left(\mathbf{n}'_{\mathrm{snap}}\right)^T\mathbf{S}_1^T\mathbf{S}_1\mathbf{n}'_{\mathrm{snap}} \approx \left(\mathbf{n}'_{\mathrm{snap}}\right)^T\mathbf{S}_2^T\mathbf{S}_2\mathbf{n}'_{\mathrm{snap}} \tag{10}$$

Using $2 \le (2-k)/(1-k)$ and Eq. (10), **P** can be rewritten as:

$$\begin{aligned} \mathbf{P} &= \mathbf{S}_1^T\mathbf{S}_2 + \mathbf{S}_2^T\mathbf{S}_1 + (2-k)/(1-k)\,\mathbf{S}_2^T\mathbf{S}_2 \\ &\approx \mathbf{S}_1^T\mathbf{S}_1 + \mathbf{S}_1^T\mathbf{S}_2 + \mathbf{S}_2^T\mathbf{S}_1 + 1/(1-k)\,\mathbf{S}_2^T\mathbf{S}_2 \\ &\ge (\mathbf{S}_1+\mathbf{S}_2)^T(\mathbf{S}_1+\mathbf{S}_2) = k^2\mathbf{S}^T\mathbf{S} \end{aligned} \tag{11}$$

Based on Eqs. (6) and (11), $SNR_{\hat{\mathbf{f}}}$can be simplified as:

$$\begin{aligned} SNR_{\hat{\mathbf{f}}} &\ge 10\log\left(\frac{\left(\mathbf{n}'_{\mathrm{snap}}\right)^T\left((1-k)^2\mathbf{S}^T\mathbf{S}+\frac{1-k}{k}k^2\mathbf{S}^T\mathbf{S}\right)\mathbf{n}'_{\mathrm{snap}}}{\left(\mathbf{n}'_{\mathrm{snap}}\right)^T\mathbf{n}'_{\mathrm{snap}}}\right) \\ &= 10\log\left(\frac{\left(\mathbf{n}'_{\mathrm{snap}}\right)^T\mathbf{S}^T\mathbf{S}\mathbf{n}'_{\mathrm{snap}}}{\left(\mathbf{n}'_{\mathrm{snap}}\right)^T\mathbf{n}'_{\mathrm{snap}}}\right) + 10\log(1-k) \end{aligned} \tag{12}$$

Furthermore, we evaluated the denoising capability of sub-Hadamard-S matrix (**S**-$\mathbf{S}_1$) in the simulation (see in Fig. 5). The simulated results indicate that the sub S-matrix could provide better

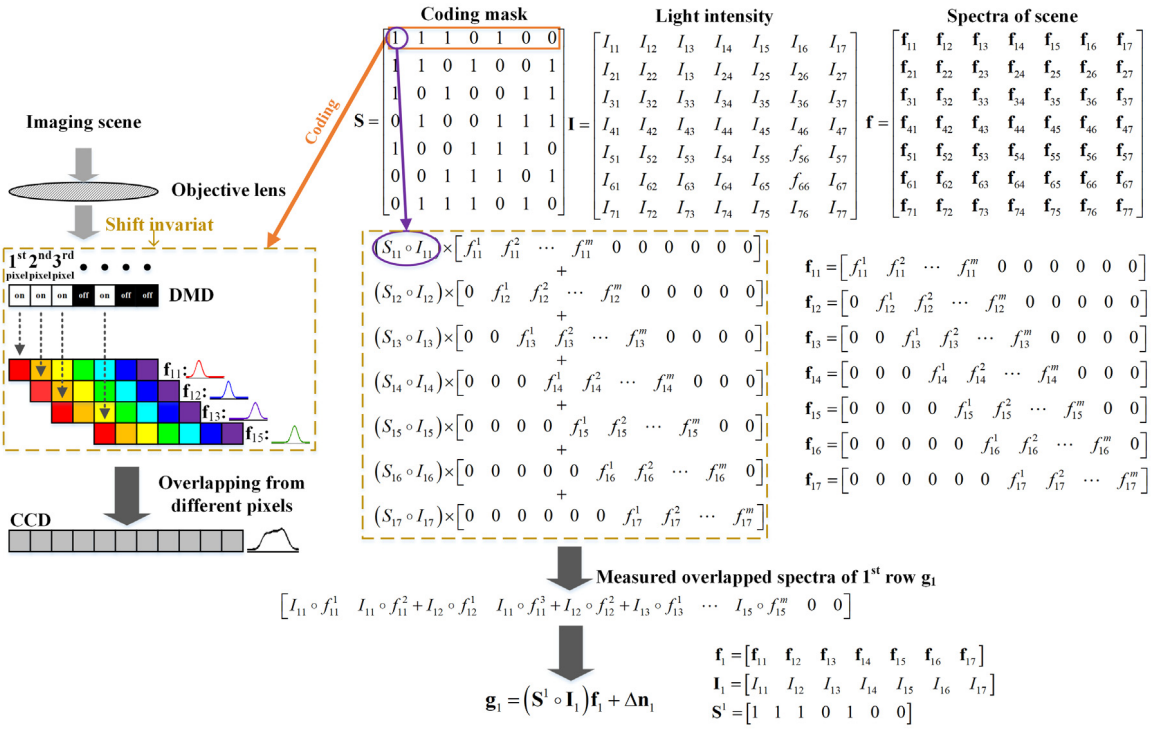

Fig. 4. Physical mechanism and mathematical expression of Hadamard-S matrix coding.

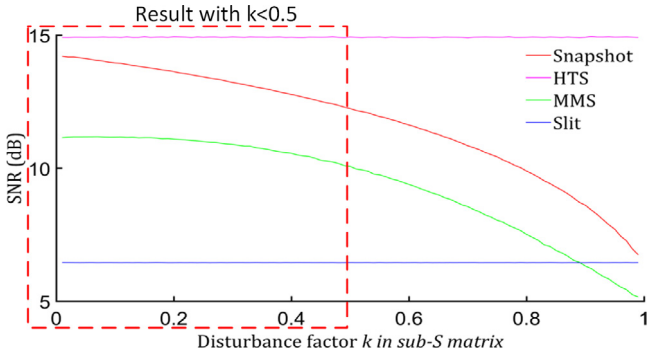

Fig. 5. Denoising capability of all methods in simulation with k along 0 to 0.99.

denoising capability and improved SNR compared with other methods such as MMS and slit.

However, the SNR of the snapshot HTS is degraded by approximately $10\log\left(\frac{1}{1-k}\right)$ (dB) with an increase in k, compared with the SNR of the traditional HTS, which satisfies Eq. (12). In the snapshot HTS, using a ground glass can further reduce the disturbance factor to below 0.5; therefore, it can achieve a more obvious SNR boost.

4. Simulation and experimental results

In this section, we present our simulated and experimental results to demonstrate the denoising capability of the sub-S matrix. Fig. 5 shows our simulated results of snapshot HTS, traditional HTS, MMS, and slit-based spectrometers, with the light intensity disturbance k in the range of 0–0.99 at an interval of 0.01. In the simulations, 127 × 127 Hadamard-S matrix is employed, the normalized solar spectrum is utilized as the original reflectance data, and white Gaussian noise is simulated as detector noise. To validate the proposed method, we repeated our simulations 100 times, and the average value is presented.

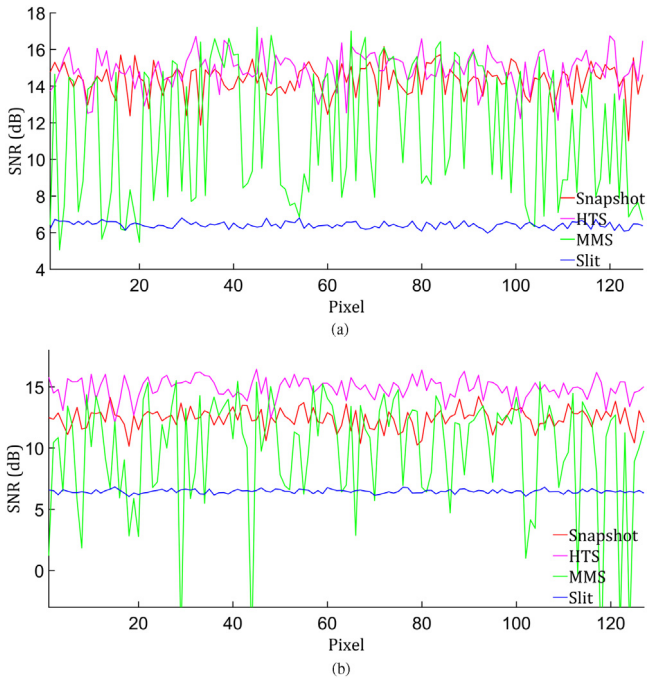

Fig. 6. Mean SNR distribution of 127 reconstructed spectra for various methods at the disturbance factor of light distribution. (a) $k = 0.1$. (b) $k = 0.5$.

In MMS, when 127 × 127 Hadamard-S matrix was employed, 127 reconstructed spectra were obtained. Because the used NNLS method belong to the so-called ill-posed inverse problem, these reconstructed spectra have different SNRs. This makes it difficult to find the highest SNR spectrum. In the simulated results, we recorded the SNR of the reconstructed spectra in each simulation and used the mean SNR boost of each spectrum and the confidence interval of all measured spectra to

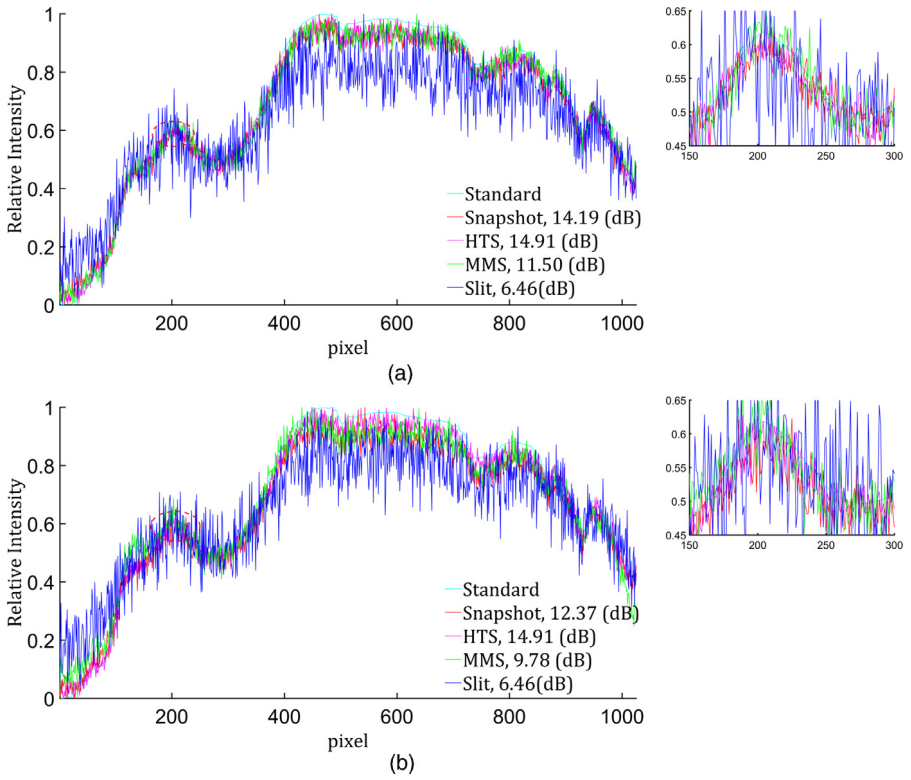

Fig. 7. Simulated results of denoising capability of the snapshot HTS, HTS, MMS and slit-based spectrometer while detector noise dominated. (a) Disturbance factor of light distribution $k = 0.1$. (b) $k = 0.5$.

Table 1
SNR range at 95% confidence interval for different methods.

	$k = 0.1$	$k = 0.5$
Snapshot	12.52–15.87	10.79–14.04
HTS	13.20–16.62	13.23–16.63
MMS	4.06–18.94	3.04–17.66
Slit	6.14–6.77	6.14–6.76

evaluate the stability of all methods. The simulated results with light intensity disturbance k of 0.1 and 0.5 are presented in Fig. 6.

As shown in Fig. 6, the SNR boost of the reconstructed spectra measured by the NNLS method at different rows is significantly different. As the disturbance of the light intensity increases, the stability of the SNR distribution degrades. In practice, for a given reconstructed spectrum with MMS, we cannot ensure its SNR boost and limit its applications. Our simulated results show that both the snapshot HTS and traditional HTS can achieve a comparable and stable SNR boost.

To compare the stability of the SNR distribution obtained by the above-mentioned methods, we employ the confidence interval to measure the stability of all methods based on the $100 \times 127 = 12{,}700$ simulated spectra. Suppose that the distribution of all simulated SNR obeys Gaussian distribution with a mean value μ and variance σ^2. According to the law of large numbers and the central limit law, the simulated results obey Gaussian distribution with the mean value μ and variance $\sigma^2/12{,}700$. In 95% confidence interval, the ranges of SNR distributions for all the methods are shown in Table 1.

As shown in Table 1, the spectra measured by the MMS shows the largest range of SNR distribution of all the methods. It can also be seen that the lower bound of the SNR boost of the MMS is the smallest of all the methods, including the slit-based spectrometer. The SNR distribution range of the snapshot HTS and traditional HTS is much smaller as compared with that of the MMS, and the lower bounds are significantly higher than that of the MMS. The slit-based spectrometer has the smallest SNR distribution range; however, its SNR boost is too small and cannot be used to measure a weak intensity signal.

We show some representative reconstructed spectra of all methods with the disturbance factor $k = 0.1, 0.5$ in Fig. 7. For the MMS, we select the spectrum with the mean SNR of all the 127 reconstructed spectra.

According to the simulated results (Fig. 7), the snapshot HTS and traditional HTS significantly outperform the slit-based spectrometer, while the detector noise dominated. Additionally, we can find that, the advantage of the snapshot HTS would decrease along with the increase of disturbance of light. When the light distribution of the scene is very smooth, the HTS and snapshot HTS have almost the same denoising capabilities. Although the intensity variation degrades the denoising performance of the snapshot HTS, it still has a significant SNR improvement. The performance of the MMS decreases with increasing light disturbance; however, as discussed earlier, the SNR boost is not stable, which limits its applications.

For evaluating the denoising capabilities of the snapshot HTS, traditional HTS, MMS, and slit-based spectrometer under experimental conditions, we measured the SNR for each method with a low-level light source. In the experiment, we use an absorptive neutral density filter to cover an LED for simulating the low-level light source. We use the slit-based spectrometer to obtain the standard spectrum with the high light of LED and long exposure time. In order to compare the performance of all methods quantitatively, we set the same exposure time in the snapshot HTS, traditional HTS, MMS, and slit-based spectrometer. For the MMS, the reconstructed spectra with the highest SNR was selected for comparison. The experimental results of all the methods are shown in Fig. 8.

In Fig. 8, 10 ms and 0 dB are the exposure time of CCD and the gain, respectively; similarly, 100 μs and 36 dB. The experimental results in Fig. 8(a) and (b) demonstrate that the snapshot HTS has better sensitivity and stability as compared with the slit-based spectrometers. Additionally, the measurement process of the snapshot HTS involves a well-defined problem; therefore, it provides better results as compared with those of the MMS. The denoising performance of the snapshot

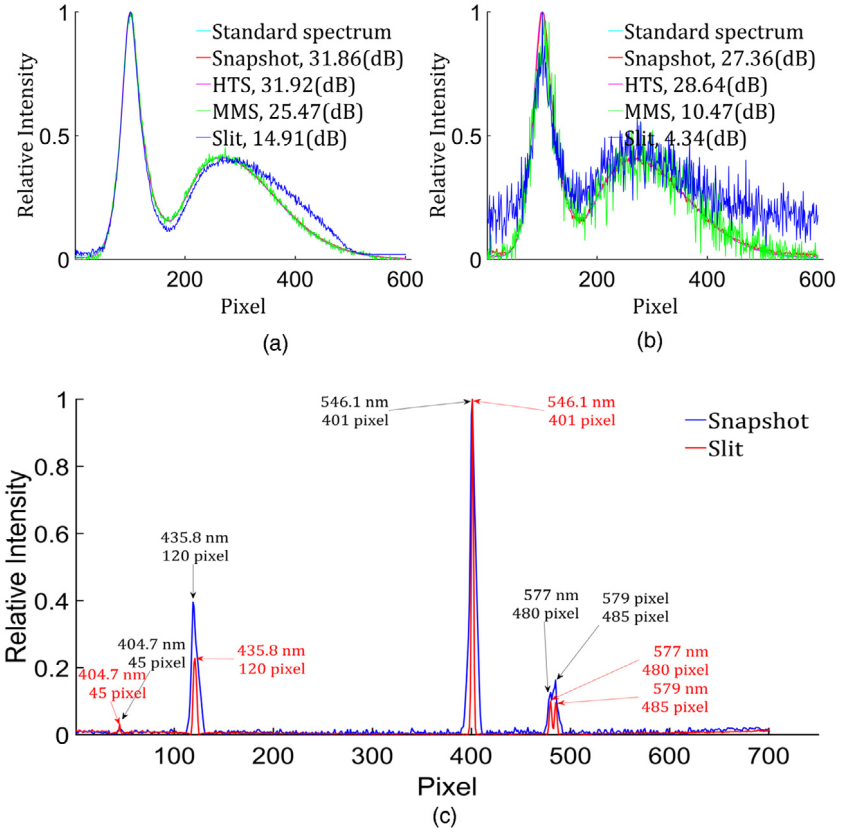

Fig. 8. Experimental results of snapshot HTS, HTS, MMS and slit-based spectrometer. (a) Experimental results with 10 ms and 0 dB. (b) Experimental results with 100 μs and 36 dB. (c) Spectrum of Hg lamp measured by snapshot HTS and slit-based spectrometer.

and the traditional HTS are observed to be at the similar level in the experiments, which indicates that the standard Hadamard-S matrix and the sub-S matrix has similar denoising capabilities.

Moreover, the Hg lamp is employed to measure the spectral resolution of the snapshot HTS and the results are shown in Fig. 8(c). The corresponding peaks (577 nm and 579 nm) positions were detected at 480th pixel and 485th pixel, respectively, which shows that the spectral resolution of the snapshot HTS is higher than 1 nm/pixel. That is, compared to the traditional silt-based spectrometer, the proposed snapshot HTS has almost the same spectral resolution.

5. Conclusion

In this paper, we propose a snapshot HTS based on the sub-Hadamard-S matrix (sub-S matrix) that has a comparable SNR boost as the traditional HTS, while maintaining the advantage of snapshot measurements, for the first time. The denoising capability of the sub-S matrix is quite robust even with the varying elements of the matrix, which makes it feasible to have high SNR. Unlike the traditional HTS, an additional imaging path has been included to collect the non-dispersed light intensity of the coded aperture in the proposed spectrometer. This allows us to use sub-S matrix coding for measurements instead of Hadamard-S matrix coding. Although, the additional imaging path increases the complexity of the system, the system can be used for the snapshot measurements and a stable SNR boost can be achieved. More importantly, unlike the snapshot spectrometers based on the convolution or compressive sensing, the proposed spectrometer involves a well-defined problem, which means the SNR boost has a certain lower bound. Compared to the slit-based spectrometer, the snapshot HTS could gain much higher SNR. Compared to the traditional HTS, the snapshot HTS can achieve comparable performance but with much higher speed. Compared to the numerical method, such as MMS and dual-camera coded aperture snapshot spectral imaging, the snapshot HTS is a well-defined problem and can obtain better and more stable results.

Declaration of competing interest

None

Acknowledgments

We thank Enlai Guo, Zhaoxin Wang for technical supports.

Funding

This work was supported by the National Natural Science Foundation of China (Grant Nos. 61727802, 61601225).

References

[1] M.E. Gehm, R. John, D.J. Brady, R.M. Willett, T.J. Schulz, Single-shot compressive spectral imaging with a dual-disperser architecture, Opt. Express 15 (2007) 14013–14027.
[2] C.V. Correa, H. Arguello, G.R. Arce, Snapshot colored compressive spectral imager, J. Opt. Soc. Amer. A 32 (2015) 1754–1763.
[3] A. Mrozack, D.L. Marks, D.J. Brady, Coded aperture spectroscopy with denoising through sparsity, Opt. Express 20 (2012) 2297–2309.
[4] A. Wagadarikar, R. John, R. Willett, D.J. Brady, Single disperser design for coded aperture snapshot spectral imaging, Appl. Opt. 47 (2008) 44–51.
[5] D. Kittle, K. Choi, A. Wagadarikar, D.J. Brady, Multiframe image estimation for coded aperture snapshot spectral imagers, Appl. Opt. 49 (36) (2010) 6824–6833.
[6] Y. Wu, I.O. Mirza, G.R. Arce, W.P. Dennis, Development of a digital-micromirror-device-based multishot snapshot spectral imaging system, Opt. Lett. 36 (14) (2011) 2692–2694.
[7] F. Kazemzadeh, A. Wong, Resolution- and throughput-enhanced spectroscopy using a high-throughput computational slit, Opt. Lett. 41 (2016) 4352–4355.

[8] X. Ma, H. Wang, Y. Wang, D. Chen, W. Chen, Q. Li, Improving the resolution and the throughput of spectrometers by a digital projection slit, Opt. Express 25 (19) (2017) 23045–23050.
[9] J. Yue, J. Han, Y. Zhang, L. Bai, High-throughput deconvolution-resolved computational spectrometer, Chin. Opt. Lett. 12 (4) (2014) 043001.
[10] M. Harwit, N.J.A. Sloane, Hadamard Transform Optics, Academic Press, 1979.
[11] M.J.E. Golay, Multi-slit spectrometry, J. Opt. Soc. Amer. 39 (1949) 437–444.
[12] M. Chi, Y. Wu, F. Qian, H. Peng, W. Zhou, Y. Liu, Signal-to-noise ratio enhancement of a Hadamard transform spectrometer using a two-dimensional slit-array, Appl. Opt. 56 (25) (2017) 7188–7193.
[13] J. Yue, J. Han, Y. Zhang, L. Bai, Denoising analysis of Hadamard transform spectrometry, Opt. Lett. 39 (2014) 3744–3747.
[14] J.A. Decker, Experimental realization of the multiplex advantage with a Hadamard-transform spectrometer, Appl. Opt. 10 (1971) 510–514.
[15] J. Yue, J. Han, L. Li, L. Bai, Denoising analysis of spatial pixel multiplex coded spectrometer with Hadamard H-matrix, Opt. Commun. 407 (2018) 355–360.
[16] A.A. Wagadarikar, M.E. Gehm, D.J. Brady, Performance comparison of aperture codes for multimodal, multiplex spectroscopy, Appl. Opt. 46 (22) (2007) 4932–4942.
[17] M.E. Gehm, S.T. McCain, N.P. Pitsianis, D.J. Brady, P. Potuluri, M.E. Sullivan, Static two-dimensional aperture coding for multimodal, multiplex spectroscopy, Appl. Opt. 45 (2006) 2965.
[18] C. Fernandez, B.D. Guenther, M.E. Gehm, D.J. Brady, M.E. Sullivan, Longwave infrared (LWIR) coded aperture dispersive spectrometer, Opt. Express 15 (9) (2007) 5742–5753.
[19] L. Wang, Z. Xiong, D. Gao, G. Shi, F. Wu, Dual-camera design for coded aperture snapshot spectral imaging, Appl. Opt. 54 (4) (2015) 848–858.
[20] J.M. Bioucas Dias, M.A.T. Figueiredo, A new TwIST: Two-step iterative shrinkage/thresholding algorithms for image restoration, IEEE Trans. Image Process. 16 (12) (2007) 2992–3004.
[21] L. Gao, R.T. Kester, N. Hagen, T.S. Tkaczyk, Snapshot image mapping spectrometer (IMS) with high sampling density for hyperspectral microscopy, Opt. Express 18 (14) (2010) 14330–14344.